NEUTRINO INTERACTIONS IN DENSE MATTER*

M. Prakash

Department of Physics & Astronomy
State University of New York at Stony Brook
Stony Brook, New York 11794-3800, U.S.A.

(Received October 29, 1999)

Even the elusive neutrinos can get trapped, but they eventually escape!

PACS numbers: 13.15.+g, 26.60.+c, 97.60.Jd

1. Introduction

Many fundamental and intrinsic properties of neutrinos play a crucial role in astrophysical phenomena such as core-collapse supernovae. Neutrinos drive supernova dynamics from beginning to end: they become trapped within the star's core early in the collapse, forming a vast energetic reservoir, and their eventual emission from the proton–neutron star is prodigious enough — containing nearly all the energy ($\sim 10^{53}$ ergs) released in the explosion — to dramatically control subsequent events. Thus investigations of both microscopic issues concerning neutrino physics in dense matter and the macroscopic consequences for supernovae, from the neutrino driven explosion to the observation of neutrinos in terrestrial detectors are needed. Among the important theoretical issues to be elucidated are:

- neutrino flavor mixing,
- ν-matter interactions including strangeness,
- strong interactions at high baryon densities via ν-matter interactions,
- the role of neutrinos in the supernova mechanism,
- the role of neutrinos in the supernova $r-$process nucleosynthesis,
- supernova relic neutrinos and cosmology.

* Presented at the XXIII International School of Theoretical Physics "Recent Developments in Theory of Fundamental Interactions", Ustroń, Poland, September 15–22, 1999.

The large neutrino flux from a proto–neutron star (PNS) plays at least two potentially important roles in the supernova environment. First, the supernova explosion itself may depend on neutrino heating to propel a shock stalled by accretion. Second, the neutrino-driven wind off the PNS that develops after shock lift-off may be a suitable site for the synthesis of heavy elements produced by the rapid neutron capture, or r-process, whose production site remains obscure. Further progress in these issues will depend upon a thorough understanding of the PNS neutrino emission.

The neutrinos of all flavors (e, μ, τ) emitted from newly formed neutron stars in supernova explosions are the only direct probe of the mechanism of supernovae and the structure of proto–neutron stars. The handful of neutrino events observed from SN 1987A [1,2] attest to this fact. More intriguingly, the three flavors of neutrino fluxes from a Galactic supernova could be distinguished by the new generation of neutrino detectors [3]. The supernova neutrino signals would furnish an opportunity to probe the properties of neutrinos and dense matter in regions that are inaccessible to terrestrial experiments.

Therefore, reliable calculations of PNS neutrino emission are an important priority. I will therefore begin by summarizing the developments to date and then point out directions for future study.

2. Evolution of proto–neutron stars

A proto–neutron star (PNS) forms in the aftermath of a successful supernova explosion as the stellar remnant becomes gravitationally decoupled from the expanding ejects. The essential microphysical ingredients that govern the macrophysical evolution of the PNS in the so-called Kelvin–Helmholtz epoch, during which the remnant changes from a hot and lepton-rich PNS to a cold and deleptonized neutron star, are the equation of state (EOS) of dense matter and its associated neutrino opacity. Among the characteristics of matter that widely vary among EOS models are their relative compressibilities (important in determining the theoretical neutron star maximum mass), symmetry energies (important in determining the typical stellar radius and in the relative n, p, e, and ν_e abundances) and specific heats (important in determining the local temperatures). These characteristics play important roles in determining the matter's composition, in particular the possible presence of strange components (such as hyperons, a kaon condensate, or quark matter). These characteristics also significantly affect calculated neutrino opacities and diffusion time scales.

The evolution of a PNS proceeds through several distinct stages [4, 5] and with various outcomes, as shown schematically in Fig. 1. Immediately following core bounce and the passage of a shock through the outer PNS's mantle, the star contains an unshocked, low entropy core of mass $M_c \simeq 0.7\ \mathrm{M}_\odot$ in which neutrinos are trapped. The core is surrounded by a low density, high entropy ($s = 5$–10) mantle that is both accreting matter falling through the shock and rapidly losing energy due to beta decays and neutrino emission. The mantle extends to the shock, which is temporarily stationary at a radius of about 200 km prior to an eventual explosion.

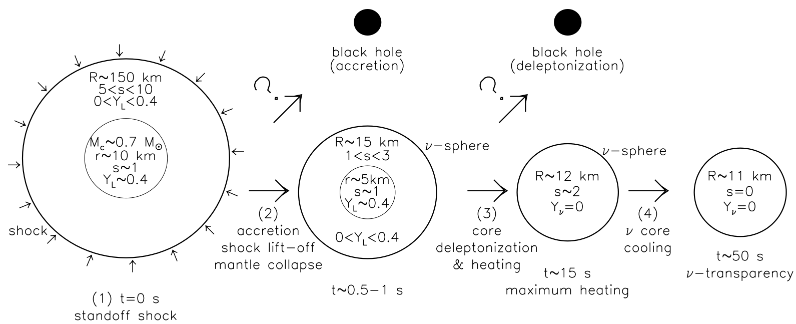

Fig. 1. The main stages of evolution of a neutron star

After a few seconds, accretion becomes less important if the supernova is successful and the shock lifts off the stellar envelope. Extensive neutrino losses and deleptonization of the mantle will have led to loss of lepton pressure and collapse of the mantle. If enough accretion occurs, the star's mass could exceed the maximum mass of the hot, lepton-rich matter and it collapses to form a black hole. In this event, neutrino emission is believed to quickly cease [6].

Neutrino diffusion deleptonizes and heats the core on time scales of 10–15 s. The core's maximum entropy is reached at the end of deleptonization. Strangeness could now appear, in which case the maximum mass will decrease, leading to another possibility of black hole formation [7]. If strangeness does not appear, the maximum mass instead increases during deleptonization and the appearance of a black hole would be less likely.

The PNS is now lepton-poor, but it is still hot. While the star has zero net neutrino number, thermally produced neutrino pairs of all flavors are abundant and dominate the emission. The star cools, the average neutrino energy decreases, and the neutrino mean free path increases. After approximately 50 seconds, the star becomes transparent to neutrinos and finally achieves a cold, catalyzed configuration.

Neutrino observations from a galactic supernova will illuminate these stages. The observables will concern time scales for deleptonization and cooling and the star's binding energy. Dimensionally, diffusion time scales are proportional to $R^2(c\lambda)^{-1}$, where R is the star's radius and λ is the effective neutrino mean free path. This generic relation illustrates how both the EOS and the composition, which determine both R and λ, influence evolutionary time scales. Additional EOS dependence enters through the rate at which the lepton number is lost from the star. The total binding energy is a stellar mass indicator.

2.1. Evolution equations

The equations that govern the transport of energy and lepton number are obtained from the Boltzmann equation for massless particles [4, 8–10]. We will focus on the non-magnetic, spherically symmetric situation. For the PNS problem, fluid velocities are small enough so that hydrostatic equilibrium is nearly fulfilled. Under these conditions, the neutrino transport equations in a stationary metric

$$ds^2 = -\mathrm{e}^{2\phi}dt^2 + \mathrm{e}^{2\Lambda}dr^2 + r^2d\theta^2 + r^2\sin^2\theta\, d\Phi^2 \tag{1}$$

are:

$$\frac{\partial(N_\nu/n_B)}{\partial t} + \frac{\partial(\mathrm{e}^{\phi}4\pi r^2 F_\nu)}{\partial a} = \mathrm{e}^{\phi}\frac{S_N}{n_B}\,, \tag{2}$$

$$\frac{\partial(J_\nu/n_B)}{\partial t} + P_\nu\frac{\partial(1/n_B)}{\partial t} + \mathrm{e}^{-\phi}\frac{\partial(\mathrm{e}^{2\phi}4\pi r^2 H_\nu)}{\partial a} = \mathrm{e}^{\phi}\frac{S_E}{n_B}\,, \tag{3}$$

where n_B is the baryon number density and a is the enclosed baryon number inside a sphere of radius r. The quantities N_ν, F_ν, and S_N are the number density, number flux and number source term, respectively, while J_ν, H_ν, P_ν, and S_E are the neutrino energy density, energy flux, pressure, and the energy source term, respectively.

In the absence of accretion, the enclosed baryon number a is a convenient Lagrangian variable. The equations to be solved split naturally into a transport part, which has a strong time dependence, and a structure part, in which evolution is much slower. Explicitly, the structure equations are

$$\frac{\partial r}{\partial a} = \frac{1}{4\pi r^2 n_B \mathrm{e}^{\Lambda}}\,, \qquad \frac{\partial m}{\partial a} = \frac{\rho}{n_B\mathrm{e}^{\Lambda}}\,, \tag{4}$$

$$\frac{\partial \phi}{\partial a} = \frac{\mathrm{e}^{\Lambda}}{4\pi r^4 n_B}\left(m + 4\pi r^3 P\right), \quad \frac{\partial P}{\partial a} = -(\rho + P)\frac{\mathrm{e}^{\Lambda}}{4\pi r^4 n_B}\left(m + 4\pi r^3 P\right). \tag{5}$$

The quantities m (enclosed gravitational mass), ρ (mass–energy density), and P (pressure) include contributions from the leptons. To obtain the equations employed in the transport, Eq. (2) may be combined with the corresponding equation for the electron fraction

$$\frac{\partial Y_e}{\partial t} = -\mathrm{e}^{\phi}\frac{S_N}{n_B} \tag{6}$$

to obtain

$$\frac{\partial Y_L}{\partial t} + \mathrm{e}^{-\phi}\frac{\partial(\mathrm{e}^{\phi}4\pi r^2 F_\nu)}{\partial a} = 0\,. \tag{7}$$

Similarly, Eq. (3) may be combined with the matter energy equation

$$\frac{dU}{dt} + P\frac{d(1/n_B)}{dt} = -\mathrm{e}^{\phi}\frac{S_E}{n_B}\,, \tag{8}$$

where U is the specific internal energy and use of the first law of thermodynamics yields

$$\mathrm{e}^{\phi}T\frac{\partial s}{\partial t} + \mathrm{e}^{\phi}\mu_\nu\frac{\partial Y_L}{\partial t} + \mathrm{e}^{-\phi}\frac{\partial \mathrm{e}^{2\phi}4\pi r^2 H_\nu}{\partial a} = 0\,, \tag{9}$$

where s is the entropy per baryon.

2.2. The equilibrium diffusion approximation

At high density and for temperatures above several MeV, the source terms in the Boltzmann equation are sufficiently strong to ensure that neutrinos are in thermal and chemical equilibrium with the ambient matter. Thus, the neutrino distribution function in these regions is both nearly Fermi–Dirac and isotropic. We can approximate the distribution function as an expansion in terms of Legendre polynomials to $O(\mu)$, which is known as the diffusion approximation. Explicitly,

$$f(\omega,\mu) = f_0(\omega) + \mu f_1(\omega)\,, \quad f_0 = [1+\mathrm{e}^{(\omega-\mu_\nu/kT)}]^{-1}\,, \tag{10}$$

where f_0 is the Fermi–Dirac distribution function at equilibrium ($T = T_{\mathrm{mat}}$, $\mu_\nu = \mu_\nu^{\mathrm{eq}}$), with ω and μ_ν being the neutrino energy and chemical potential, respectively. The main goal is to obtain a relation for f_1 in terms of f_0. In the diffusion approximation, one obtains [10]

$$f_1 = -D(\omega)\left[\mathrm{e}^{-\Lambda}\frac{\partial f_0}{\partial r} - \omega \mathrm{e}^{-\Lambda}\frac{\partial \phi}{\partial r}\frac{\partial f_0}{\partial \omega}\right]\,. \tag{11}$$

The explicit form of the diffusion coefficient D appearing above is given by

$$D(\omega) = \left(j + \frac{1}{\lambda_a} + \kappa_1^s\right)^{-1}\,. \tag{12}$$

The quantity $j = j_a + j_s$, where j_a is the emissivity and j_s is the scattering contribution to the source term. The absorptivity is denoted by λ_a and κ_1^s is the well-known transport opacity. Substituting

$$\frac{\partial f_0}{\partial r} = -\left(T\frac{\partial \eta_\nu}{\partial r} + \frac{\omega}{T}\frac{\partial T}{\partial r}\right)\frac{\partial f_0}{\partial \omega}\,, \tag{13}$$

where $\eta_\nu = \mu_\nu/T$ is the neutrino degeneracy parameter, in Eq. (11), we obtain

$$f_1 = -D(\omega)\mathrm{e}^{-\Lambda}\left[T\frac{\partial \eta}{\partial r} + \frac{\omega}{T\mathrm{e}^{\phi}}\frac{\partial (T\mathrm{e}^{\phi})}{\partial r}\right]\left(-\frac{\partial f_0}{\partial \omega}\right). \tag{14}$$

Thus, the energy-integrated lepton and energy fluxes are

$$\begin{aligned} F_\nu &= -\frac{\mathrm{e}^{-\Lambda}\mathrm{e}^{-\phi}T^2}{6\pi^2}\left[D_3\frac{\partial (T\mathrm{e}^{\phi})}{\partial r} + (T\mathrm{e}^{\phi})D_2\frac{\partial \eta}{\partial r}\right], \\ H_\nu &= -\frac{\mathrm{e}^{-\Lambda}\mathrm{e}^{-\phi}T^3}{6\pi^2}\left[D_4\frac{\partial (T\mathrm{e}^{\phi})}{\partial r} + (T\mathrm{e}^{\phi})D_3\frac{\partial \eta}{\partial r}\right]. \end{aligned} \tag{15}$$

The coefficients D_2, D_3, and D_4 are related to the energy-dependent diffusion coefficient $D(\omega)$ through

$$D_n = \int_0^\infty dx\; x^n D(\omega) f_0(\omega)(1 - f_0(\omega))\,, \tag{16}$$

where $x = \omega/T$. These diffusion coefficients depend only on the microphysics of the neutrino-matter interactions (see §4 for details). The fluxes appearing in the above equations are for one particle species. To include all six neutrino types, we redefine the diffusion coefficients in Eq. (15):

$$D_2 = D_2^{\nu_e} + D_2^{\bar\nu_e}\,, \quad D_3 = D_3^{\nu_e} - D_3^{\bar\nu_e}\,, \quad D_4 = D_4^{\nu_e} + D_4^{\bar\nu_e} + 4D_4^{\nu_\mu}\,. \tag{17}$$

2.3. Flux limiters

In regions of small optical depth, diffusion codes can predict fluxes that exceed the black-body limit. To prevent this, the fluxes are corrected by a flux limiter $3\Lambda(\xi)$, where $\xi_F = F_\nu/N_\nu$ and $\xi_H = H_\nu/J_\nu$ for the number and energy fluxes, respectively. For the functional form of $\Lambda(\xi)$, both the Levermore & Pomraning [11] and the Bowers & Wilson [12] flux-limiters have been tested. Only the outermost few mass shells are affected by this choice which does not make an appreciable difference in the overall evolution or in the mean neutrino energies or luminosities.

The structure equations (4) and (5) satisfy the boundary conditions

$$\begin{aligned} r(a=0) &= 0; \quad m(a=0)=0, \\ \phi(a=a_s) &= \frac{1}{2}\log\left[1-\frac{2m(a=a_s)}{r(a=a_s)}\right]; \quad P(a=a_s)=P_s\,, \end{aligned} \tag{18}$$

where a_s is the total number of baryons in the star, which remains fixed during the evolution, and P_s is the surface pressure, which is chosen to be very small. Usually, results are insensitive to the exact value of P_s. The transport Eqs (7) and (9) also require boundary conditions. Both the energy and number fluxes must be zero at the center. At the surface, we may write $\xi_F = \alpha_n$ and $\xi_H = \alpha_e$, where α_n and α_e are constants chosen each to be in the range 0.4–0.6. The neutrino number and energy fluxes are insensitive to the exact choice of these constants, due to the fact that the fluxes saturate near the surface and the values of Y_ν in the surface region adjusts itself to compensate for small changes in α_n and α_e.

2.4. Neutrino luminosities

A fair representation of the signal in a terrestrial detector can be found from the time dependence of the total neutrino luminosity and average neutrino energy together with an assumption of a Fermi–Dirac spectrum with zero chemical potential. We will return to discuss the improvements necessary to obtain more accurate information about the spectra.

The total neutrino luminosity is the time rate of change of the star's gravitational mass, and is therefore primarily a global property of the evolution. This luminosity, due to energy conservation, must also equal

$$L_\nu = \mathrm{e}^{2\phi} 4\pi r^2 H_\nu \tag{19}$$

at the edge of the star. This relation serves as a test of energy conservation, at least for all times greater than about 5 ms, when the star comes into radiative equilibrium. For times greater than about 5 ms, initial transients become quite small and the predicted luminosities should be relatively accurate compared to full transport simulation. Estimate of the average energy of neutrinos is made from the temperature T_ν of the matter at the neutrinosphere R_ν, defined to be the location in the star where the flux factor $\xi_H = 0.25$. However, since the spectrum may not be Fermi–Dirac at the neutrinosphere, a diffusion scheme cannot give a very precise value for the average energy. Comparing with better transport in this region, one finds that the average energy $\langle E_\nu \rangle \approx 3T_\nu$, where T_ν is a mass average in the outermost zone. Because it is a globally determined quantity, the luminosity L_ν is necessarily more accurately determined than either R_ν or T_ν.

3. The equation of state

The masses and radii of neutron stars depend upon the matters' compressibility, the composition of matter at high density, and the nuclear symmetry energy (*e.g.*, [7]). In the PNS problem, the finite temperature aspects of the EOS also play an important role. During the early evolution the entropy in the central regions is moderately high, $s \sim 1$–2 (in units of Boltzmann's constant), which correspond to temperatures in the range $T = 20$–50 MeV. These features may be explored by employing a finite temperature field-theoretical model in which the interactions between baryons are mediated by the exchange of σ, ω, and ρ mesons. The hadronic Lagrangian density is given by [13]

$$\begin{aligned} L_H \;=\; & \sum_i \overline{B_i}(-i\gamma^\mu\partial_\mu - g_{\omega i}\gamma^\mu\omega_\mu - g_{\rho i}\gamma^\mu \boldsymbol{b}_\mu\cdot\boldsymbol{t} - M_i + g_{\sigma i}\sigma)B_i \\ & -\frac{1}{4}W_{\mu\nu}W^{\mu\nu} + \frac{1}{2}m_\omega^2\omega_\mu\omega^\mu - \frac{1}{4}\boldsymbol{B}_{\mu\nu}\boldsymbol{B}^{\mu\nu} + \frac{1}{2}m_\rho^2 b_\mu b^\mu \\ & +\frac{1}{2}\partial_\mu\sigma\partial^\mu\sigma - \frac{1}{2}m_\sigma^2\sigma^2 - U(\sigma)\,. \end{aligned} \tag{20}$$

Here, B are the Dirac spinors for baryons and $\mathbf{t}$ is the isospin operator. The sums include baryons $i = n, p, \Lambda, \Sigma$, and Ξ. The field strength tensors for the ω and ρ mesons are $W_{\mu\nu} = \partial_\mu\omega_\nu - \partial_\nu\omega_\mu$ and $\boldsymbol{B}_{\mu\nu} = \partial_\mu\boldsymbol{b}_\nu - \partial_\nu\boldsymbol{b}_\mu$, respectively. The potential $U(\sigma)$ represents the self-interactions of the scalar field and is taken to be of the form [14]

$$U(\sigma) = \frac{1}{3}bM_n(g_{\sigma N}\sigma)^3 + \frac{1}{4}c(g_{\sigma N}\sigma)^4\,. \tag{21}$$

The partition function Z_H for the hadronic degrees of freedom is evaluated in the mean field approximation. The total partition function $Z_{\rm total} = Z_H Z_L$, where Z_L is the standard noninteracting partition function of the leptons. Using $Z_{\rm total}$, the thermodynamic quantities can be obtained in the standard way. The additional conditions needed to obtain a solution are provided by the charge neutrality requirement, and, when neutrinos are trapped, the set of equilibrium chemical potential relations required by the general condition

$$\mu_i = b_i\mu_n - q_i(\mu_l - \mu_{\nu_\ell})\,, \tag{22}$$

where b_i is the baryon number of particle i and q_i is its charge. The introduction of additional variables, the neutrino chemical potentials, requires additional constraints, which we supply by fixing the lepton fractions, $Y_{L\ell}$, appropriate for conditions prevailing in the evolution of the PNS. In addition to models containing only nucleonic degrees of freedom (GM1np & GM3np) we investigate models that allow for the presence of hyperons (GM1npH & GM3npH). For the determination of the various coupling constants appearing in Z_H see [7].

Thermal effects contribute only modestly to the total pressure. The pressure is dominated from effects of interactions and degeneracy at high density. While the differences between lepton rich and lepton poor matter for the np models are negligible, significant differences arise in models with hyperons. When the electron neutrino fraction is large, their presence inhibits the appearance of hyperons. Note however, that a large hyperonic component at high density in the neutrino free case significantly softens the EOS [7]. This softening with decreasing lepton number will lead to compression during the deleptonization epoch. Hence, there exists a window of initial masses for which the star becomes unstable to gravitational collapse during deleptonization. The maximum masses supported at low temperature and for lepton poor matter are significantly smaller than for hot and lepton rich matter.

Finite temperature properties of matter at high density influence the diffusion of neutrinos especially through the specific heat. Neutrino mean free paths are strongly temperature dependent (see §4) and the ambient matter temperature controls the diffusion of neutrinos to a large extent. In the left panel of Fig. 2, we show the matter temperature at fixed entropy per baryon as a function of the baryon density to contrast the behavior observed in models with and without hyperons. The trends observed in the np models are similar while the differences between np and npH models are very significant. The appearance of hyperons increases the low temperature specific heat. This generally favors lower temperatures during the evolution for the npH models, all else being equal. This is because, in charge neutral and beta-equilibrated matter, bulk of the entropy resides in the baryons [7]. Under degenerate situations ($T/E_{F_i} \gg 1$), this result may be understood from the relation that connects the temperature and baryonic entropy (or specific heat) through the concentrations ($Y_i = n_i/n$):

$$\frac{\pi^2 T}{s} = \frac{(3\pi^2 n_B)^{2/3}}{\sum_i Y_i^{1/3}\sqrt{M_i^{\star 2} + k_{F_i}^2}} \Rightarrow \begin{cases} \dfrac{(3\pi^2 n_B)^{2/3}}{\sum_i Y_i^{1/3} M_i^\star} & \text{for } M_i^\star \gg k_{F_i} \\ \dfrac{(3\pi^2 n_B)^{1/3}}{\sum_i Y_i^{2/3}} & \text{for } M_i^\star \ll k_{F_i}\,, \end{cases} \tag{23}$$

where $k_{F_i} = (3\pi^2 n_B Y_i)^{1/3}$ are the Fermi momenta. For the temperatures of interest here, and particularly with increasing density, the above relation provides an accurate representation of the exact results for entropies per baryon even up to $s = 2$. The behavior with density of both the concentrations and effective masses controls the temperatures for a fixed s. In the absence of any variation with $M_i^\star$, a system with more components at a given baryon density has a smaller temperature than a system with fewer components (recall that $\sum_i Y_i = 1$). Effective masses that rapidly drop with density oppose this behavior and lead to larger temperatures. The fact that the temperatures are smaller in the presence of hyperons than those in nucleons-only matter attests to the predominant effect of concentrations. Note that the differences between the temperatures for the cases with and without hyperons are larger than those obtained by using different models for the individual cases.

However, the appearance of hyperons also leads to higher central densities due to softening; this acts to compensate for the higher specific heat in npH models. In addition, the larger neutrino chemical potentials in npH models generate larger entropies during the deleptonization epoch; this also acts to increase the central temperature in these models. Results clearly show that despite the significant differences seen in Fig. 2 the maximum central temperatures reached in the both np and npH models are nearly equal due to the above mentioned feedbacks.

The lepton chemical potentials influence the deleptonization epoch. For np models a lower nuclear symmetry energy favors a larger ν_e fraction and has little effect on the e^- fraction at $Y_l = 0.4$. Models with hyperons lead to significantly larger μ_{ν_e} and lower μ_e, both of which influence the diffusion of

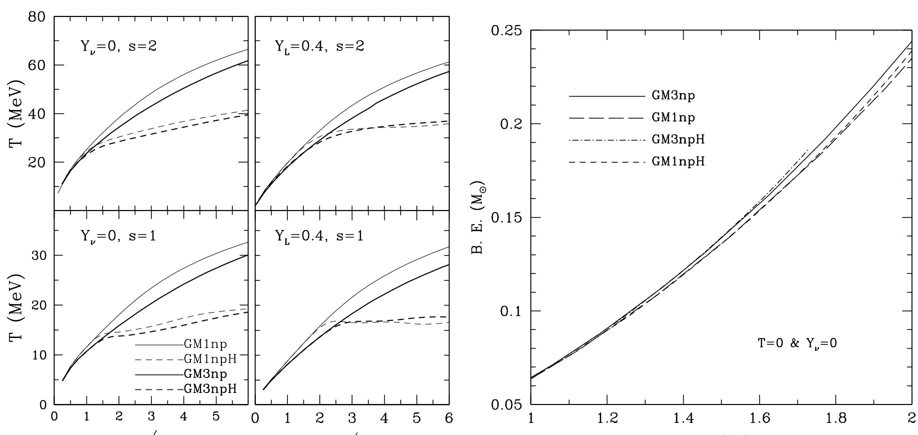

Fig. 2. Left: Temperatures attained in lepton-poor (left) and lepton-rich (right) matter at finite entropy as a function of baryon density n_B (n_0 is the nuclear equilibrium density). The symbol np refers to matter with nucleons-only and npH to matter including hyperons. Right: Binding energy as a function of baryon mass. The symbol np refers to matter with nucleons-only and npH to matter including hyperons at T=0 and Y$_\nu$=0.

electron neutrinos. The electron chemical potentials in neutrino free matter are reduced to a greater extent by changes in composition and symmetry energy as there are no neutrinos to compensate for changes in $\hat{\mu} = \mu_n - \mu_p$.

The binding energy (B.E.), which is a global aspect of the energetics, is the difference between baryonic and gravitational masses, and is an important observational parameter because nearly 99% of it appears as radiated neutrino energy. The rate of change of binding is essentially the total neutrino luminosity. Figure 2 displays B.E. versus baryonic mass for the models considered here. There exists a universal empirical relationship between the B.E. and the mass [7,15]:

$$\text{B.E.} = (M_B - M_G)c^2 \simeq (0.065 \pm 0.01)\ (M_B/\mathrm{M}_\odot)^2\ \mathrm{M}_\odot\,. \tag{24}$$

This universality is not greatly altered by the presence of significant softening due to the presence of hyperons, kaons or quarks. Since nearly all of the B.E. is released in the form of neutrinos, *an accurate measurement of the total neutrino energy will lead to a good estimate of the remnant mass.* However, as the results of Fig. 2 show, it will not be possible to distinguish the various EOSs from the total B.E. alone.

4. Neutrino-matter interaction rates

One of the important microphysical inputs in PNS simulations is the neutrino opacity at supra-nuclear density [4,16–20]. Although it was realized over a decade ago that the effects due to degeneracy and strong interactions significantly alter the neutrino mean free paths, it is only recently that detailed calculations have become available [21–28]. The scattering and absorption reactions that contribute to the neutrino opacity are

$$\nu_e + B \ \rightarrow\ e^- + B'\,, \qquad \bar{\nu}_e + B \rightarrow e^+ + B'\,, \tag{25}$$

$$\nu_X + B \ \rightarrow\ \nu_X + B'\,, \qquad \nu_X + e^- \rightarrow \nu_X + e^-\,, \tag{26}$$

where the scattering reactions are common to all neutrino species and the dominant source of opacity for the electron neutrinos is due to the charged reaction. The weak interaction rates in hot and dense matter are modified due to many in-medium effects. The most important of these are:

(1) *Composition*: The neutrino mean free paths depend sensitively on the composition which is sensitive to the nature of strong interactions. First, the different degeneracies of the different Fermions determines the single-pair response due to Pauli blocking. Second, neutrinos couple differently to different baryonic species; consequently, the net rates will depend on the individual concentrations.

(2) *In-medium dispersion relations*: At high density, the single-particle spectra are significantly modified from their noninteracting forms due to effects of strong interactions. Interacting matter features smaller effective baryon masses and energy shifts relative to non-interacting matter.

(3) *Correlations*: Repulsive particle–hole interactions and Coulomb interactions generally result in a screened dielectric response and also lead to collective excitations in matter. These effects may be calculated using the Random Phase Approximation (RPA), in which ring diagrams are summed to all orders. Model calculations [21,23,25,29–34] indicate that at high density the neutrino cross sections are suppressed relative to the case in which these effects are ignored. In addition, these correlations enhance the average energy transfer in neutrino–nucleon collisions. Improvements in determining the many-body dynamic form factor and assessing the role of particle–particle interactions in dense matter at finite temperature are necessary before the full effects of many-body correlations may be ascertained.

(4) *Axial charge renormalization*: In dense matter, the axial charge of the baryons is renormalized [35–37], which alters the neutrino–baryon couplings from their vacuum values. Since the axial contribution to the scattering and absorption reactions is typically three times larger than the vector contributions, small changes in the axial vector coupling constants significantly affect the cross sections. The calculation of this renormalization requires a theoretical approach which treats the pion and chiral symmetry breaking explicitly. So far, this has been done in isospin symmetric nuclear matter [38], but not for neutron matter or for beta-equilibrated neutron star matter. Substantial reductions may be expected in the ν-matter cross sections from this in-medium effect.

(5) *Multi-Pair excitations*: Neutrinos can also excite many-particle states in an interacting system, inverse bremsstrahlung being an example of a two-particle excitation [39]. These excitations provide an efficient means of transferring energy between the neutrinos and baryons which are potentially significant in low-density matter. However, multigroup neutrino transport will be needed to include this effect. In addition, such calculations require source terms for neutrino processes such as bremsstrahlung and neutrino pair production. The latter process has been accurately treated in [40].

The relative importance of the various effects described above on neutrino transport is only beginning to be studied systematically. As a first step, we will focus on effects due to modifications (1) through (3) above.

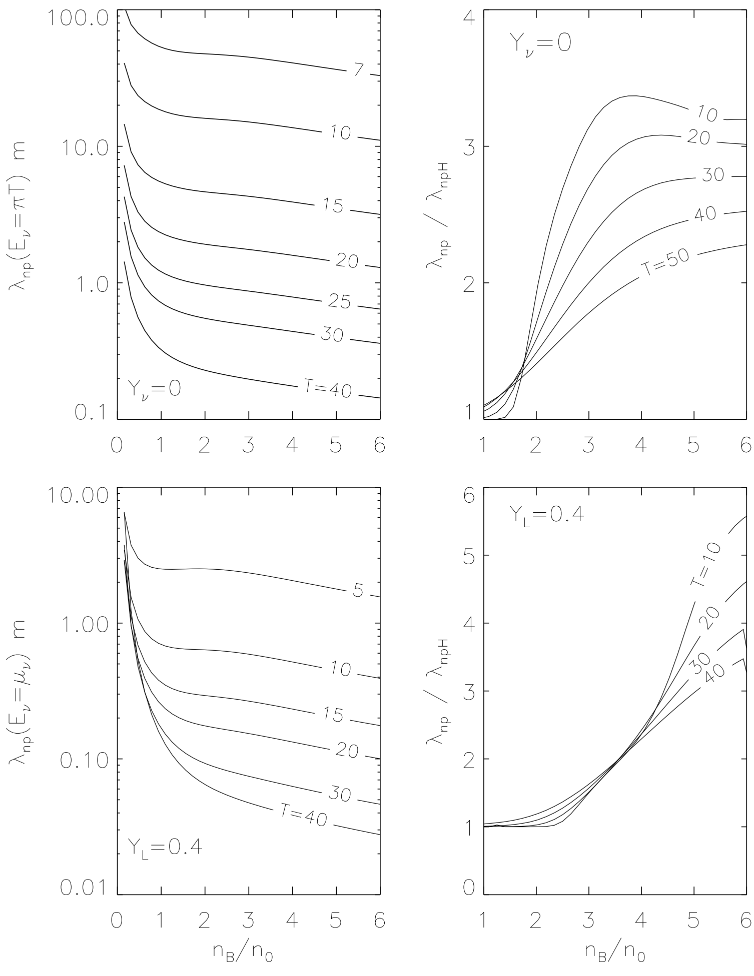

Fig. 3. Neutrino mean free paths in matter with nucleons only (left panels). Right panels show ratios of mean free paths in matter without and with hyperons. Abscissa is baryon density n_B (n_0 is the nuclear equilibrium density). Top panels show scattering mean free paths common to all neutrino species. The bottom panels show results for electron neutrino mean free paths where absorption reactions are included. The neutrino content is labelled in the different panels.

Under degenerate conditions even modest changes to the composition significantly alter the neutrino scattering and absorption mean free paths. In Fig. 3, the neutrino scattering and absorption mean free paths are shown for models GM3np and GM3npH relevant to the deleptonization and cooling epochs. The top panels show the scattering mean free paths common to all neutrino species in neutrino free matter. The scattering mean free paths for thermal neutrinos ($E_\nu = \pi T$) is shown in the left panel for various temperatures. To study the influence of hyperons, the ratio of the $\lambda_{\rm np}/\lambda_{\rm npH}$ is shown in the right panels. The presence of hyperons significantly increase the scattering cross sections, by a factor $\sim$ (2–3). Similar results for the absorption cross sections are shown in the lower panels for $Y_L = 0.4$. Again we notice a significant enhancement (right panel) when hyperons appear, the factor here could be as large as 5.

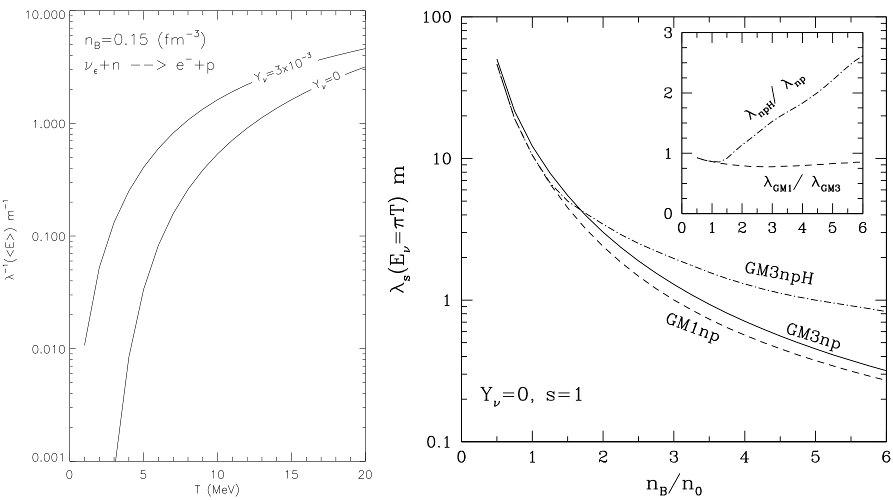

Fig. 4. Left: Charged current inverse neutrino mean free paths versus temperature. Right: Comparison of scattering mean free paths in neutrino poor matter at fixed entropy for different EOSs in matter containing nucleons and also hyperon.

During the deleptonization stage, lepton number transport is sensitive to charged current reactions which dominate scattering reactions. At zero temperature, charged current reactions $\nu + n \leftrightarrow e + p$ depend sensitively on the proton fraction Y_p [41]. Kinematic restrictions require Y_p to be larger than 11–14% (direct Urca threshold). At early times, a finite neutrino chemical potential favors a large Y_p throughout the star, which enables these reactions to proceed without any hindrance. Toward the late stages, however, Y_p decreases with decreasing μ_ν and charged current reactions may be naively expected to become inoperative. The threshold density for the charged current reaction when $\mu_\nu = 0$ and $T = 0$ depends sensitively on the density dependence of the nuclear symmetry energy. In field-theoretical models, in which the symmetry energy is largely given by contributions due to ρ-meson exchange, the critical density is typically $n_B = 2 \sim 3n_0$. However, finite temperatures favor larger Y_p's and increase the average neutrino energy enabling the charged current reactions to proceed even below these densities. Figure 4 shows that this is the case even at relatively low temperatures ($T \sim$ 3–5) MeV for a baryon density $n_B = 0.15$ fm^{-3}. The sharp rise with temperature, which occurs even for $Y_\nu = 0$, clearly indicates that this reaction dominates the ν_e opacity even during the late deleptonization era. Thus, charged current reactions cannot be simply turned off when the neutrino chemical potential becomes small enough as was done in prior PNS simulations [4].

The EOS and neutrino mean free paths are intimately related, which is best illustrated by comparing the results shown in Fig. 3 with those shown in Fig. 4. Composition and the baryon effective masses influence both the neutrino mean free paths and the matter's specific heat. Hyperons decrease the neutrino mean free paths at constant temperature (Fig. 3). This trend is reversed at constant entropy due to the significantly lower temperatures favored in npH matter. Similar effects are apparent when we compare np models with different baryon effective masses. At a constant temperature, the larger effective mass in model GM3np favors larger cross sections, while at constant entropy this trend is again reversed due to the lower temperatures favored by the larger specific heat.

The diffusion coefficients are calculated using Eq. (16) with the cross sections discussed above. The diffusion coefficients D_2, D_3, and D_4 are functions of n_B, T, and Y_{ν_e}.

5. Results and discussion

Neutrino emission from PNS's depends on many stellar properties, including the mass; initial entropy, lepton fraction and density profiles; and neutrino opacities. Pons et al. [10] carried out a detailed study of the dependence of neutrino emission on PNS characteristics. They verified the generic results of Burrows & Lattimer [4] that both neutrino luminosities and average energies increased with increasing mass (see Fig. 5). In addition, they found that variations in initial entropy and lepton fraction profiles in the outer regions of the PNS caused only transient (lasting a few tenths of a second) variations in neutrino luminosities and energies. Variations in the central lepton fraction and entropy were found to produce modest changes in neutrino luminosities that persisted to late times. The central values of lepton fraction and entropy are established during core collapse, and will depend upon the initial properties of the star as well as the EOS and neutrino transport during the collapse.

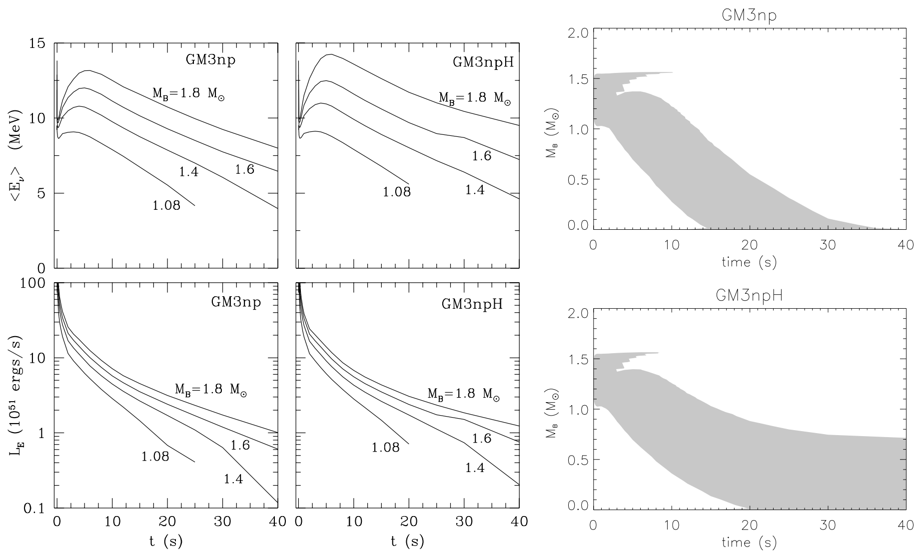

Fig. 5. Left: The evolution of the neutrino average energy and total neutrino luminosity is compared for several assumed PNS baryon masses and EOSs. The EOSs in the left panels contain only baryons and leptons while those in the right panels also contain hyperons. Right: The regions of PNS which are unstable to convection by the Ledoux–Schwarzschild criterion as a function of time are shown as shaded areas. Two EOSs are compared: without hyperons (top panel) and with hyperons (bottom panel).

Properties of the dense matter EOS that affect PNS evolution include the compressibility, symmetry energy, specific heat, and composition. Pons *et al.* [10] employed a field theoretical EOS [7], with which the results due to some differences in stellar size (due to variations in nuclear interactions) and composition were studied. Some results are summarized in Fig. 5. Overall, both the average energies and luminosities of stars containing hyperons were larger compared to those without. In addition, for stars without hyperons, those stars with smaller radii had higher average emitted neutrino energy, although the predicted luminosities for early times ($t < 10$ s) were insensitive to radii. This result only holds if the opacities are calculated consistently with each EOS [24,25]; otherwise rather larger variations in evolutions would have been found [20, 27]. The same held true for models which allowed for the presence of hyperons, except when the initial proto–neutron star mass was significantly larger than the maximum mass for cold, catalyzed matter. Another new result was that the average emitted neutrino energy of all flavors increased during the first 5 seconds of evolution, and then decreased nearly linearly with time. For times larger than about 10 seconds, and prior to the occurrence of neutrino transparency, the neutrino luminosities decayed exponentially with a time constant that was sensitive to the high-density properties of matter. Significant variations in neutrino emission occurred beyond 10 seconds: it was found that neutrino luminosities were larger during this time for stars with smaller radii and with the inclusion of hyperons in the matter. Finally, significant regions of the stars appeared to become convectively unstable during the evolution (see Fig. 5), as several works have found [42–45].

5.1. Influence of many-body correlations

The main effect of the larger mean free paths produced by RPA corrections [25] is that the inner core deleptonizes more quickly. In turn, the maxima in central temperature and entropy are reached on shorter timescales. In addition, the faster increase in thermal pressure in the core slows the compression associated with the deleptonization stage, although after 10 s the net compressions of all models converge.

The relatively large, early, changes in the central thermodynamic variables do not, however, translate into similarly large effects on observables such as the total neutrino luminosity and the average radiated neutrino energy, relative to the baseline simulation. The luminosities for the different models are shown as a function of time in Fig. 6. The left panel shows the early time development in detail. The exploratory models agree with the results reported in [27, 28]. However, the magnitude of the effects when full RPA corrections are applied is somewhat reduced compared to the exploratory models. It is especially important that at and below nuclear density, the corrections due to correlations are relatively small. Since information from the inner core is transmitted only by the neutrinos, the time scale to propagate any high density effect to the neutrinosphere is the neutrino diffusion time scale. Since the neutrinosphere is at a density approximately $1/100$ of nuclear density, and large correlation corrections occur only above $1/3$ nuclear density where nuclei disappear, we find that correlation corrections calculated here have an effect at the neutrinosphere only after 1.5 s. Moreover, the RPA suppresion we have calculated is considerably smaller than those reported in [27, 28], reaching a maximum of about 30% after 5 s, compared to a luminosity increase of 50% after only 2 s. However, the corrections are still very important during the longer-term cooling stage (see Fig. 6), and result in a more rapid onset of neutrino transparency compared to the Hartree results.

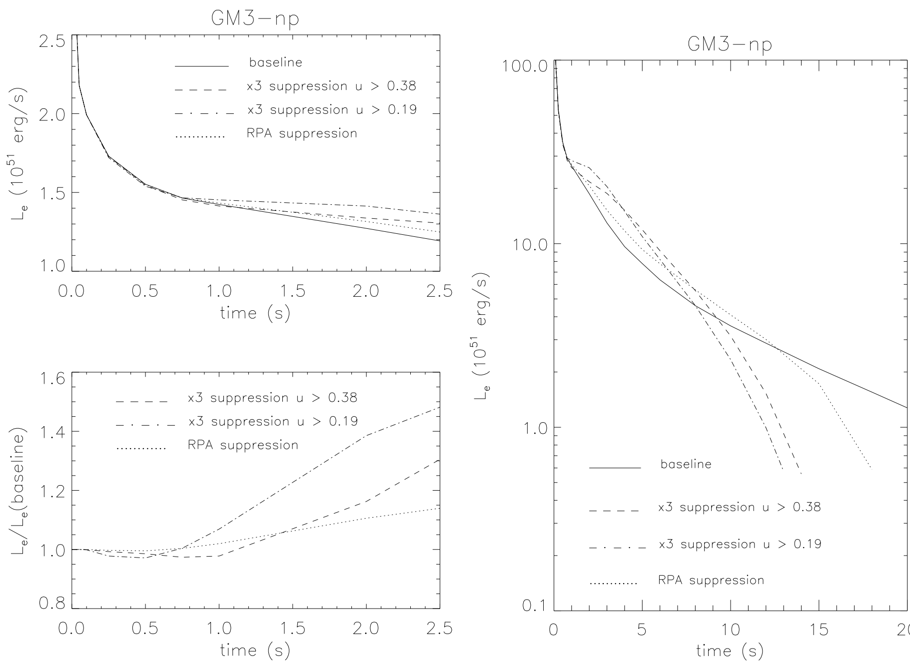

Fig. 6. Left: The upper panel shows the total emitted neutrino luminosity for the PNS evolutions described in Reddy et al. [25]. The lower panel shows the ratio of the luminosities obtained in the three models which contain corrections to the baseline (Hartree approximation) model. Right: Emitted neutrino luminosity for long-term PNS evolutions.

6. Outlook

I turn now to physics issues which merit further attention. The reader is urged to supplement this list with his or her own items.

6.1. Dynamic structure functions from microscopic calculations

Neutrino properties of astrophysical interest depend crucially on the nature of the excitation spectrum of the nuclear medium to spin and spin–isospin probes. The excited states are very different depending upon whether or not interactions in the medium conserve spin and spin–isospin. The importance of tensor correlations in the medium is thus clear, since they break the conservation laws. Friman & Maxwell [46] first emphasized the importance of tensor correlations in the process

$$\nu_e + n + n \to e^- + p + n \,, \tag{27}$$

and noted that their neglect underestimates the rate of ν_e absorption by as much as an order of magnitude. In their study, they used a hard core description of the short range correlations and a one pion exchange model for the medium and long range ones. Sawyer & Soni [47] and Haensel & Jerzak [48], who used additional correlations based on a Reid soft core potential, confirmed that large reductions were possible in degenerate matter for non-degenerate neutrinos.

Since these earlier works, many-body calculations have vastly improved (*e.g.* [49]) and have been well-tested against data on light nuclei and nuclear matter. Much better tensor correlations are now available, so that we may better pin down the rate of absorption due to the above process. Detailed calculations to include arbitrary matter and neutrino degeneracies encountered in many astrophysical applications are necessary.

6.2. Coherent scattering in novel phases of matter

A first order phase transition at high baryon density implies that a mixed phase can occupy a significant region of the interior of a neutron star [50]. Reddy, Bertsch & Prakash [26] have recently investigated the effect of a droplet phase on neutrino transport inside the core. The coherent scattering of neutrinos off the large weak charge in the droplets greatly increases the neutrino opacity of the mixed phase. The reduction of the mean free path compared to that in pure neutron matter could be as large as one to two orders of magnitude. The presence of a first order phase transition is thus likely to have a dramatic and discernible effect on the temporal characteristics of supernova neutrino light curves. It would be interesting to explore the effects arising from a first order phase transition during the evolution of a PNS. This entails a delineation of the mixed phase including the possible existence of more complicated structures than simple droplets. These studies will provide contrasts with those in which normal nucleonic matter and hyperonic matter were considered.

6.3. π^- and K^- Dispersion relations through ν-nucleus reactions

The experimental program that would do the most to illuminate theoretical issues permeating neutrino interactions in dense matter would be studies of neutrino reactions on heavy nuclei, the only direct way of probing the matrix elements of the axial current in nuclear matter. Pioneering suggestions in this regard have been put forth by Sawyer & Soni [51, 52], Ericson [53], and Sawyer [54]. The basic idea is to detect positively charged leptons (μ^+ or e^+) produced in inclusive experiments

$$\bar{\nu} + X \;\rightarrow\; \mu^+ \text{ (or } e^+) \; + \pi^- \text{ (or } K^-) + X \tag{28}$$

which is kinematically made possible when the in-medium π^- or K^- dispersion relation finds support in space-like regions. The sharp peaks at forward angles in the differential cross section versus lepton momentum survive the 100–200 MeV width in the incoming GeV or so neutrinos from accelerator experiments. Calculations of the background from quasi-elastic reactions indicate that the signal would be easily detectable.

6.4. Relic neutrinos from past supernovae and cosmological models

Type II supernovae have occurred everywhere in the universe since galaxies began to form. The diffuse neutrino background from such supernovae, the so-called relic neutrinos, thus offer an opportunity to look back into cosmological evolution [55, 56]. The Super-Kamiokande detector is currently in a position to record relic $\bar{\nu}_e$'s up to 50 MeV or so. Comparisons with theoretical predictions are, however, necessary to disentangle cosmological information from characteristics that are solely due spectral features of supernova neutrinos, which depend both on the progenitor star mass and the range of possible PNS masses. An equally important factor is the supernova formation rate, which in turn depends on the initial mass function of stars capable of producing core collapse supernovae. Explicitly, the differential flux of relic supernova $\bar{\nu}_e$'s at the present epoch is given by

$$\frac{dF_\nu}{dq} = c \int_z^0 dz\, R_{SN}(z) \frac{dN(q(1+z))}{dq} (1+z) \frac{dt}{dz}\,, \tag{29}$$

where c is a constant, z is the redshift, q is the neutrino energy, $R_{SN}(z)$ is the supernova formation rate, $dN(q(1+z))/dq$ is a weighted average of the number of neutrinos of energy q per unit q, and the factor dt/dz accounts for the cosmological evolution. Estimates of the relic flux performed to date [57–62] have focused on the uncertainties stemming from those residing in the factors R_{SN} and dt/dz. The supernova formation rate at the present time, derived from observed supernovae, radio pulsar data, statistics on stellar types and nucleosynthesis, is uncertain, lying in the range 0.02–0.1 per year per galaxy. There is also uncertainty concerning its z dependence. The cosmological evolution, studied through the Friedmann equation, depends on both Ω_0 ($= \rho_0/\rho_c$, ρ being the matter energy density) and the cosmological constant Λ, with weak sensitivity to Λ. The weighted average of the neutrino number spectrum per unit energy has been deduced from ref. [57], and is typically assumed to be Fermi–Dirac in character.

Luminosities issuing from PNS's show great sensitivity to the PNS mass and the dense matter EOS. The energy spectra will depend upon details of neutrino transport both in the diffusive and semi-transparent regimes. Thus, more reliable spectra (dN/dq) than available to date, and more realistic estimates of the total neutrino energy emitted as a function of stellar mass would be useful. With these inputs, we may examine critically the relic neutrino background.

It is a pleasure to thank James Lattimer, Juan Miralles, Jose Pons, and Sanjay Reddy, with whom the work reported here was performed. I thank Adam Burrows and Ray Sawyer for many lively and beneficial discussions. Finally, I thank Henryk Czyz and the local organizing committee, particularly the young guys and gals who took care of me oh so well, for their warm and cheerful hospitality. This work was supported in part by the U.S. Department of Energy under grant number DOE/DE-FG02-88ER-40388 and by the NASA grant NAG52863.

REFERENCES

[1] R.M. Bionta *et al.*, *Phys. Rev. Lett.* **58**, 1494 (1987).
[2] K. Hirata *et al.*, *Phys. Rev. Lett.* **58**, 1490 (1987).
[3] A. Burrows, D. Klein, R. Gandhi, *Phys. Rev.* **D45**, 3361 (1992).
[4] A. Burrows, J.M. Lattimer, *Astrophys. J.* **307**, 178 (1986).
[5] A. Burrows, *Ann. Rev. Nucl. Sci.* **40**, 181 (1990).
[6] A. Burrows, *Astrophys. J.* **334**, 891 (1988).
[7] M. Prakash, I. Bombaci, Manju Prakash, P.J. Ellis, J.M. Lattimer, R. Knorren, *Phys. Rep.* **280**, 1 (1997).
[8] R.W. Lindquist, *Ann. Phys.* **37**, 478 (1966).
[9] K.S. Thorne, *Mon. Not. R. Astron. Soc.* **194**, 439 (1981).
[10] J.A. Pons, S. Reddy, M. Prakash, J.M. Lattimer, J.A. Miralles, *Astrophys. J.* **513**, 780 (1999).
[11] C.D. Levermore, G.C. Pomraning, *Astrophys. J.* **248**, 321 (1981).
[12] R.L. Bowers, J.R. Wilson, *Astrophys. J. Supp.* **50**, 115 (1982).
[13] B.D. Serot, J.D. Walecka, in *Advances in Nuclear Physics*, Vol. 16, eds J.W. Negele & E. Vogt, Plenum, New York 1986, p.1.
[14] N.K. Glendenning, S. Moszkowski, *Phys. Rev. Lett.* **67**, 2414 (1991).
[15] J.M. Lattimer, A. Yahill, *Astrophys. J.* **340**, 426 (1989).
[16] S.W. Bruenn, *Astrophys. J. Supp.* 58, 771 (1985).
[17] A. Mezzacappa, S.W. Bruenn, 1993, *Astrophys. J.*, 405, 637
[18] J.R. Wilson, R.W. Mayle, in *The Nuclear Equation of State Part A*, eds W. Greiner and H. Stöcker, Plenum, New York, 1989, p.731.
[19] H. Suzuki, K. Sato, in *The Structure and Evolution of Neutron Stars,* eds D. Pines, R. Tamagaki, and S. Tsuruta, Addison-Wesley, New York 1992, p.276.

[20] W. Keil, H.T. Janka, *Astron. Astrophys.* **296**, 145 (1995).

[21] S. Reddy, J. Pons, M. Prakash, J.M. Lattimer, in *Stellar Evolution, Stellar Explosions and Galactic Chemical Evolution*, ed. T. Mezzacappa, IOP Publishing, Bristol 1997, p.585

[22] S. Reddy, M. Prakash, *Astrophys. J.* **423**, 689 (1997).

[23] M. Prakash, S. Reddy, in *Nuclear Astrophysics*, eds M. Buballa, W. Nörenberg, J. Wambach and A. Wirzba, GSI, Darmstadt 1997, p.187.

[24] S. Reddy, M. Prakash, J.M. Lattimer, *Phys. Rev.* **D58**, 013009 (1998).

[25] S. Reddy, M. Prakash, J.M. Lattimer, J.A. Pons, *Phys. Rev.* **C59**, 2888 (1999).

[26] S. Reddy, G. Bertsch, M. Prakash, nucl-th/9909040, 1999.

[27] A. Burrows, R.F. Sawyer, *Phys. Rev.* **C58**, 554 (1998).

[28] A. Burrows, R.F. Sawyer, *Phys. Rev.* **C59**, 510 (1999).

[29] R.F. Sawyer, *Phys. Rev.* **D11**, 2740 (1975).

[30] R.F. Sawyer, *Phys. Rev.* **C40**, 865 (1989).

[31] N. Iwamoto, C.J. Pethick, *Phys. Rev.* **D25**, 313 (1982).

[32] C.J. Horowitz, K. Wehrberger, *Nucl. Phys.* **A531**, 665 (1991a); *Phys. Rev. Lett.*, **66**, 272 (1991b); *Phys. Lett.* **B226**, 236 (1992).

[33] G. Raffelt, D. Seckel, *Phys. Rev.* **D52**, 1780 (1995).

[34] G. Sigl, *Phys. Rev. Lett.* **76**, 2625 (1996).

[35] D.H. Wilkinson, *Phys. Rev.* **C7**, 930 (1973).

[36] M. Rho, *Nucl. Phys.* **A231**, 493 (1974).

[37] G.E. Brown, M. Rho, *Phys. Rev. Lett.* **66**, 2720 (1991).

[38] G. Carter, P.J. Ellis, S. Rudaz, *Nucl. Phys.* **A603**, 367 (1996).

[39] S. Hannestad, G. Raffelt, *Astrophys. J.* **507**, 339 (1998).

[40] J.A. Pons, J.A. Miralles, J.-M. Ibañez, *Astron. & Astrophys. Supp.* **129**, 343 (1998).

[41] J.M. Lattimer, C.J. Pethick, M. Prakash, P. Haensel, *Phys. Rev. Lett.*, **66**, 2701 (1991).

[42] A. Burrows, B. Fryxell, *Astrophys. J. Lett.* **413**, L33 (1993).

[43] M. Herant, W. Benz, J. Hicks, C. Fryer, S.A. Colgate, *Astrophys. J.* **425**, 339 (1994).

[44] W. Keil, H.T. Janka, E. Müller, *Astrophys. J.* **473**, L111 (1995).

[45] A. Mezzacappa, A.C. Calder, S.W. Bruenn, J.M. Blondin, M.W. Guidry, M.R. Strayer, A.S. Umar, *Astrophys. J.* **495**, 911 (1998).

[46] B. Friman, O. Maxwell, *Astrophys. J.* **232**, 541 (1979).

[47] R.F. Sawyer, A. Soni, *Astrophys. J.* **230**, 859 (1979).

[48] P. Haensel, A.J. Jerzak, *Astron. Astrophys.* **179**, 127 (1987).

[49] A. Akmal, V.R. Pandharipande, *Phys. Rev.* **C24**, 2261 (1997).

[50] N.K. Glendenning, *Phys. Rev.* **D46**, 1274 (1992).

[51] R.F. Sawyer, A. Soni, *Phys. Rev. Lett.* **38**, 1383 (1977).

[52] R.F. Sawyer, A. Soni, *Phys. Rev.* **C18**, 898 (1978).

[53] M. Ericson, *Nucl. Phys.* **A518**, 116 (1990).

[54] R.F. Sawyer, *Phys. Rev. Lett.* **73**, 3363 (1994).

[55] G.S. Bisnovatyi-Kogan, S.F. Deidov, *Ann. N. Y. Acad. Sci.* **422**, 319 (1984).

[56] L.M. Krauss, S.L. Glashow, D.N. Schramm, *Nature* **310**, 191 (1984).

[57] S.E. Woosley, J.R. Wilson, R. Mayle, *Astrophys. J.* **302**, 19 (1986).

[58] Y. Totsuka, *Rep. Prog. Phys.* **55**, 377 (1992).

[59] H. Suzuki, in *Physics and Astrophysics of Neutrinos*, eds M. Fukugita and A. Suzuki, Springer-Verlag, 1994, p.763.

[60] T. Totani, K. Sato, Y. Yoshii, *Astrophys. J.* **460**, 303 (1996).

[61] R.A. Malaney, *Astropart. Phys.* **7**, 125 (1997).

[62] D.H. Hartmann, S.E. Woosley, *Astropart. Phys.* **7**, 137 (1997).